Opto-Electronic Advances

Supplementary information

2021, Vol. 4, No. 12

DOI: 10.29026/oea.2021.210027

Robust far-field imaging by spatial coherence engineering

Yonglei Liu[1,2], Yahong Chen[3], Fei Wang[3]*, Yangjian Cai[1,2,3]*, Chunhao Liang[1,2]* and Olga Korotkova[4]

[1]Shandong Provincial Engineering and Technical Center of Light Manipulations & Shandong Provincial Key Laboratory of Optics and Photonic Device, School of Physics and Electronics, Shandong Normal University, Jinan 250014, China; [2]Collaborative Innovation Center of Light Manipulations and Applications, Shandong Normal University, Jinan 250358, China; [3]School of Physical Science and Technology, Soochow University, Suzhou 215006, China; [4]Department of Physics, University of Miami, Coral Gables, Florida 33146, USA.

*Correspondence: F Wang, E-mail: fwang@suda.edu.cn; YJ Cai, E-mail: yangjiancai@suda.edu.cn; CH Liang, E-mail: Cliang@dal.ca

This file includes:

Supplementary information for this paper is available at https://doi.org/10.29026/oea.2021.210027

Section 1: Derivation of the cross-spectral density function of a cosine-Gaussian correlated Schell-model beam propagating through an ABCD optical system

In this section, we derive the cross-spectral density (CSD) function of a cosine-Gaussian correlated Schell-model (CGC-SM) beam with a cross phase (CP), propagating in a paraxial ABCD optical system, and obtain the condition of the recovery of the modulus of degree of coherence (DOC) function in the far field. The CSD function of such beam in the source plane is expressed as

$$W_0(\boldsymbol{r}_1,\boldsymbol{r}_2)=\exp\left(-\frac{\boldsymbol{r}_1^2+\boldsymbol{r}_2^2}{4{\omega_0}^2}\right)\mu_0(\Delta\boldsymbol{r})\exp\left[\mathrm{i}u\left(x_1y_1-x_2y_2\right)\right]\ , \tag{S1}$$

where u is the strength factor. ω_0 denotes the beam width. $\boldsymbol{r}_i=(x_i,y_i)$, $(i=1,2)$ are two arbitrary position vectors in the source plane. The function $\mu_0(\Delta\mathbf{r})$ denotes the DOC, given by

$$\mu_0(\Delta\boldsymbol{r})=\cos\left(\frac{n\sqrt{2\pi}\Delta x}{\delta_0}\right)\cos\left(\frac{n\sqrt{2\pi}\Delta y}{\delta_0}\right)\exp\left(-\frac{\Delta\boldsymbol{r}^2}{2\delta_0^2}\right)\ . \tag{S2}$$

n and δ_0 in Eq. S2 are the beam order and transverse coherence width, respectively. $\Delta\boldsymbol{r}=\boldsymbol{r}_1-\boldsymbol{r}_2=(\Delta x,\Delta y)$ is the difference of two position vectors.

Within the accuracy of paraxial approximation, the propagation of the CSD function in a paraxial ABCD optical system can be treated by the extended Collins integral:

$$W(\boldsymbol{\rho}_1,\boldsymbol{\rho}_2)=\frac{k^2}{4\pi^2B^2}\exp\left[-\frac{\mathrm{i}kD}{2B}\left(\boldsymbol{\rho}_1^2-\boldsymbol{\rho}_2^2\right)\right]\int\int_{-\infty}^{\infty}W_0(\boldsymbol{r}_1,\boldsymbol{r}_2)\exp\left[-\frac{\mathrm{i}kA}{2B}\left(\boldsymbol{r}_1^2-\boldsymbol{r}_2^2\right)\right]\exp\left[\frac{\mathrm{i}k}{B}\left(\boldsymbol{r}_1\cdot\boldsymbol{\rho}_1-\boldsymbol{r}_2\cdot\boldsymbol{\rho}_2\right)\right]\mathrm{d}^2\boldsymbol{r}_1\mathrm{d}^2\boldsymbol{r}_2\ , \tag{S3}$$

where A, B and D are the elements of the transfer matrix of an optical system, k is the wavenumber, $\boldsymbol{\rho}_i=(\rho_{ix},\rho_{iy})$,$(i=1,2)$ are two arbitrary position vectors in the receiver plane.

Then, we insert Eq. S2 into Eq. S1 then into Eq. S3, and introduce the following "sum" and "difference" coordinates,and introduce the following "sum" and "difference" coordinates,

$$\begin{aligned}\boldsymbol{r}_s&=\left(\boldsymbol{r}_1+\boldsymbol{r}_2\right)/2\ ,\ \Delta\boldsymbol{r}=\boldsymbol{r}_1-\boldsymbol{r}_2\ ,\\ \boldsymbol{\rho}_s&=\left(\boldsymbol{\rho}_1+\boldsymbol{\rho}_2\right)/2\ ,\ \Delta\boldsymbol{\rho}=\boldsymbol{\rho}_1-\boldsymbol{\rho}_2\ .\end{aligned} \tag{S4}$$

After tedious but straightforward integrating, we obtain the expression for the CSD function in the receiver plane

$$\begin{aligned}W(\boldsymbol{\rho}_1,\boldsymbol{\rho}_2)\ =\ &\frac{\sqrt{1-h^2}k^2\omega_0^2}{2B^2M}\exp\left(-\frac{a^2}{M}\right)\exp\left(-\mathrm{i}\frac{Dk}{M}\boldsymbol{\rho}_s\cdot\Delta\boldsymbol{\rho}\right)\exp\left(-\frac{k^2\omega_0^2}{2B^2}\Delta\boldsymbol{\rho}^2\right)\exp\left[\frac{k^2}{2B^2M}\left(\rho_{yx}^2+\rho_{xy}^2+2h\rho_{xy}\rho_{yx}\right)\right]\\ &\times\left\{\exp\left[\frac{\mathrm{i}ak}{BM}\left(\rho_{xy}+h\rho_{yx}\right)\right]\cos\left[\frac{ak}{BM}\left(\rho_{yx}+h\rho_{xy}\right)+\frac{\mathrm{i}a^2h}{M}\right]+\exp\left[-\frac{\mathrm{i}ak}{BM}\left(\rho_{xy}+h\rho_{yx}\right)\right]\right.\\ &\left.\cdot\cos\left[\frac{ak}{BM}\left(\rho_{yx}+\ h\rho_{xy}\right)-\frac{\mathrm{i}a^2h}{M}\right]\right\}\ ,\end{aligned} \tag{S5}$$

with

$$\begin{aligned}&\Omega^2=\frac{1}{4\omega_0^2}+\frac{1}{{\delta_0}^2},\ h=\frac{2Auk\omega_0^2}{B\left(\Omega^2+\omega_0^2u^2+A^2k^2\omega_0^2/B^2\right)},M=\left(\Omega^2+\omega_0^2u^2+A^2k^2\omega_0^2/B^2\right)\left(1-h^2\right),\\ &a=\frac{n\sqrt{2\pi}}{\delta_0},\ \rho_{\alpha\beta}=\mathrm{i}\rho_{s\alpha}+\frac{A\omega_0^2k}{B}\Delta\rho_\alpha-u\omega_0^2\Delta\rho_\beta,\ \ (\alpha,\beta=x,y)\ .\end{aligned} \tag{S6}$$

Equation S5 is too rather complicated to obtain the closed form of the DOC during propagation. Let us consider a typical focusing system: a lens with focal length f is inserted into the source plane, and the receiver plane is at the distance z after the Lens. In this case, the elements of the transfer matrix are

$$\begin{pmatrix}A&B\\C&D\end{pmatrix}=\begin{pmatrix}1&z\\0&1\end{pmatrix}\begin{pmatrix}1&0\\-1/f&1\end{pmatrix}=\begin{pmatrix}1-z/f&z\\-1/f&1\end{pmatrix}\ . \tag{S7}$$

If the receiver plane is just in the rear focal plane of the lens, i.e., A=0, B=f, and D=1, the CSD function is then simplified as

$$W(\boldsymbol{\rho}_1,\boldsymbol{\rho}_2) = \frac{k^2\omega_0^2}{f^2M_0}\exp\left(-\frac{a^2}{M_0}\right)\exp\left(-\mathrm{i}\frac{k}{f}\boldsymbol{\rho}_s\cdot\Delta\boldsymbol{\rho}\right)\exp\left(-\frac{k^2\omega_0^2\Omega^2}{2f^2M_0}\Delta\rho^2\right)\exp\left[-\frac{\mathrm{i}u\omega_0^2k^2}{f^2M_0}\left(\Delta\rho_x\rho_{sy}+\Delta\rho_y\rho_{sx}\right)\right]$$
$$\times\exp\left(-\frac{k^2}{2f^2M_0}\rho_s^{\,2}\right)\cos\left[\frac{ak}{fM_0}\left(\mathrm{i}\rho_{sx}-u\omega_0^2\Delta\rho_y\right)\right]\cos\left[\frac{ak}{fM_0}\left(\mathrm{i}\rho_{sy}-u\omega_0^2\Delta\rho_x\right)\right], \tag{S8}$$

where $M_0=\Omega^2+\omega_0^2u^2$ and $\Delta\boldsymbol{\rho}=\boldsymbol{\rho}_1-\boldsymbol{\rho}_2=(\Delta\rho_x,\Delta\rho_y)$.

By applying the following relation

$$\cos(a\pm b)=\cos a\cos b\mp\sin a\sin b\,, \tag{S9}$$

the last three terms in Eq. S8 are expanded as

$$\begin{aligned}
&\exp\left(-\frac{k^2}{2f^2M_0}\rho_s^2\right)\cos\left[\frac{ak}{fM_0}\left(\mathrm{i}\rho_{sx}-u\omega_0^2\Delta\rho_y\right)\right]\cos\left[\frac{ak}{fM_0}\left(\mathrm{i}\rho_{sy}-u\omega_0^2\Delta\rho_x\right)\right]\\
&=\exp\left[-\left(\frac{k\rho_{sx}}{f\sqrt{2M_0}}\right)^2\right]\cosh\left(\alpha\frac{k\rho_{sx}}{f\sqrt{2M_0}}\right)\exp\left[-\left(\frac{k\rho_{sy}}{f\sqrt{2M_0}}\right)^2\right]\cosh\left(\alpha\frac{k\rho_{sy}}{f\sqrt{2M_0}}\right)\cos\left(\frac{u\omega_0^2ak}{fM_0}\Delta\rho_y\right)\cos\left(\frac{u\omega_0^2ak}{fM_0}\Delta\rho_x\right)\\
&+\exp\left[-\left(\frac{k\rho_{sx}}{f\sqrt{2M_0}}\right)^2\right]\sinh\left(\alpha\frac{k\rho_{sx}}{f\sqrt{2M_0}}\right)\exp\left[-\left(\frac{k\rho_{sy}}{f\sqrt{2M_0}}\right)^2\right]\cosh\left(\alpha\frac{k\rho_{sy}}{f\sqrt{2M_0}}\right)\sin\left(\frac{u\omega_0^2ak}{fM_0}\Delta\rho_y\right)\cos\left(\frac{u\omega_0^2ak}{fM_0}\Delta\rho_x\right)\\
&+\exp\left[-\left(\frac{k\rho_{sx}}{f\sqrt{2M_0}}\right)^2\right]\cosh\left(\alpha\frac{k\rho_{sx}}{f\sqrt{2M_0}}\right)\exp\left[-\left(\frac{k\rho_{sy}}{f\sqrt{2M_0}}\right)^2\right]\sinh\left(\alpha\frac{k\rho_{sy}}{f\sqrt{2M_0}}\right)\cos\left(\frac{u\omega_0^2ak}{fM_0}\Delta\rho_y\right)\sin\left(\frac{u\omega_0^2ak}{fM_0}\Delta\rho_x\right)\\
&+\exp\left[-\left(\frac{k\rho_{sx}}{f\sqrt{2M_0}}\right)^2\right]\sinh\left(\alpha\frac{k\rho_{sx}}{f\sqrt{2M_0}}\right)\exp\left[-\left(\frac{k\rho_{sy}}{f\sqrt{2M_0}}\right)^2\right]\sinh\left(\alpha\frac{k\rho_{sy}}{f\sqrt{2M_0}}\right)\sin\left(\frac{u\omega_0^2ak}{fM_0}\Delta\rho_y\right)\sin\left(\frac{u\omega_0^2ak}{fM_0}\Delta\rho_x\right),
\end{aligned} \tag{S10}$$

with $\alpha=a\sqrt{2/M_0}$.

In Eq. S10, we assume that the condition (a), i.e., $\alpha\ll1$ is satisfied, implying that the cosh function and sinh function in Eq. S10 are about 1 and 0, respectively, in the range of the Gaussian function with increasing value. Under this circumstance, Eq. S10 reduces to

$$\begin{aligned}
&\exp\left(-\frac{k^2}{2f^2M_0}\boldsymbol{\rho}_s^2\right)\cos\left[\frac{ak}{fM_0}\left(\mathrm{i}\rho_{sx}-u\omega_0^2\Delta\rho_y\right)\right]\cos\left[\frac{ak}{fM_0}\left(\mathrm{i}\rho_{sy}-u\omega_0^2\Delta\rho_x\right)\right]\\
&\approx\exp\left[-\left(\frac{k\rho_{sx}}{f\sqrt{2M_0}}\right)^2\right]\exp\left[-\left(\frac{k\rho_{sy}}{f\sqrt{2M_0}}\right)^2\right]\cos\left(\frac{u\omega_0^2ak}{fM_0}\Delta\rho_y\right)\cos\left(\frac{u\omega_0^2ak}{fM_0}\Delta\rho_x\right).
\end{aligned} \tag{S11}$$

Hence Eq. S8 reduces

$$W(\boldsymbol{\rho}_1,\boldsymbol{\rho}_2) = \frac{k^2\omega_0^2}{f^2M_0}\exp\left(-\frac{a^2}{M_0}\right)\exp\left(-\mathrm{i}\frac{k}{f}\boldsymbol{\rho}_s\cdot\Delta\boldsymbol{\rho}\right)\exp\left(-\frac{k^2\omega_0^2\Omega^2}{2f^2M_0}\Delta\boldsymbol{\rho}^2\right)\exp\left[-\frac{\mathrm{i}u\omega_0^2k^2}{f^2M_0}\left(\Delta\rho_x\rho_{sy}+\Delta\rho_y\rho_{sx}\right)\right]$$
$$\times\exp\left[-\left(\frac{k\rho_{sx}}{f\sqrt{2M_0}}\right)^2\right]\exp\left[-\left(\frac{k\rho_{sy}}{f\sqrt{2M_0}}\right)^2\right]\cos\left(\frac{u\omega_0^2ak}{fM_0}\Delta\rho_y\right)\cos\left(\frac{u\omega_0^2ak}{fM_0}\Delta\rho_x\right), \tag{S12}$$

with the condition (a), we derive

$$a\sqrt{2/M_0}\ll1\,, \tag{S13}$$

namely,

$$u>\frac{\sqrt{200a^2-\Omega^2}}{\omega_0}\,. \tag{S14}$$

According to the definition of the DOC, the modulus of the DOC in the focal plane takes the form

$$\begin{aligned}
\left|\mu_f(\boldsymbol{\rho}_1-\boldsymbol{\rho}_2)\right| &= \frac{|W(\boldsymbol{\rho}_1,\boldsymbol{\rho}_2)|}{\sqrt{W(\boldsymbol{\rho}_1,\boldsymbol{\rho}_1)W(\boldsymbol{\rho}_2,\boldsymbol{\rho}_2)}}\\
&=\left|\exp\left[-\frac{1}{2\delta_f^2}(\boldsymbol{\rho}_1-\boldsymbol{\rho}_2)^2\right]\cos\left[\frac{\sqrt{2\pi}n}{\sqrt{M_0/\omega_0^2u^2}\delta_f}\left(\rho_{1x}-\rho_{2x}\right)\right]\cos\left[\frac{\sqrt{2\pi}n}{\sqrt{M_0/\omega_0^2u^2}\delta_f}\left(\rho_{1y}-\rho_{2y}\right)\right]\right|,
\end{aligned} \tag{S15}$$

with

$$u_f = \frac{\omega_0^2 k^2}{f^2 M_0} u \ , \tag{S16}$$

$$\omega_f = \frac{f}{k}\sqrt{M_0} \ , \tag{S17}$$

$$\delta_f = \frac{f\delta_0}{k\omega_0}\sqrt{M_0} \ . \tag{S18}$$

The u_f, ω_f, and δ_f are the CP strength factor, beam width, and coherence width in the focal plane, respectively. Now we assume the condition (b) $\sqrt{M_0/\omega_0^2 u^2} \to 1$, namely.

$$u > \sqrt{10}\Omega/\omega_0 \ . \tag{S19}$$

The DOC described by Eq. S15 reduces to

$$\left|\mu_f(\boldsymbol{\rho}_1 - \boldsymbol{\rho}_2)\right| = \left|\exp\left[-\frac{1}{2\delta_f^2}(\boldsymbol{\rho}_1 - \boldsymbol{\rho}_2)^2\right]\cos\left[\frac{\sqrt{2\pi}n}{\delta_f}\left(\rho_{1x} - \rho_{2x}\right)\right]\cos\left[\frac{\sqrt{2\pi}n}{\delta_f}\left(\rho_{1y} - \rho_{2y}\right)\right]\right| \ , \tag{S20}$$

with $\delta_f = (fu/k)\,\delta_0$. It follows from Eq. S20 that under the conditions (a) and (b), the DOC function in the focal plane (far field) becomes the same form with that [shown in Eq. S2] in the source plane, except for the coherence width is δ_f instead of δ_0. Finally, the conditions (a) and (b) are combined as the following form

$$u > \max\left\{\frac{\sqrt{200a^2 - \Omega^2}}{\omega_0}, \frac{\sqrt{10}\Omega}{\omega_0}\right\} \ . \tag{S21}$$

Section 2: Image retrieval by Fienup's phase retrieval (FPR) algorithms

Fienup[1,2] proposed the phase retrieval algorithms, which can retrieve an image from the magnitude of the spatial Fourier spectrum only by using a priori information of the object, such as being real or non-negative.

The basics of Fienup's phase retrieval (FPR) algorithms are shown in Fig. S1. The algorithm starts with an initial guess $P_1(x, y)$ of the object. When a low resolutions image of the object is available, this image is a logical choice for the initial guess. Otherwise, a completely random pattern can be used to start the algorithm. The initial guess is entered into an algorithm that performs the following four steps at its k^{th} iteration

$$\begin{aligned}
&\text{step1}: \ \mu_k(u,v) = FT\{P_k(x,y)\}\,, \\
&\text{step2}: \ \theta_k(u,v) \ = arg\{\mu_k(u,v)\}\,, \\
&\text{step3}: \ \mu_k'(u,v) = |\mu_m|\, e^{i\theta_k(u,v)}, \\
&\text{step4}: \ P_k'(x,y) = IFT\{\mu_k'(u,v)\} \ ,
\end{aligned} \tag{S22}$$

where we use the information from the measurement of the module of the DOC in the third step. At this point the algorithm requires real space constraints on the object. In our case, the object of P has to be real and positive. We define a set Γ that contains all the points in P_k violating this constraint; in our case the points with a negative or complex value.

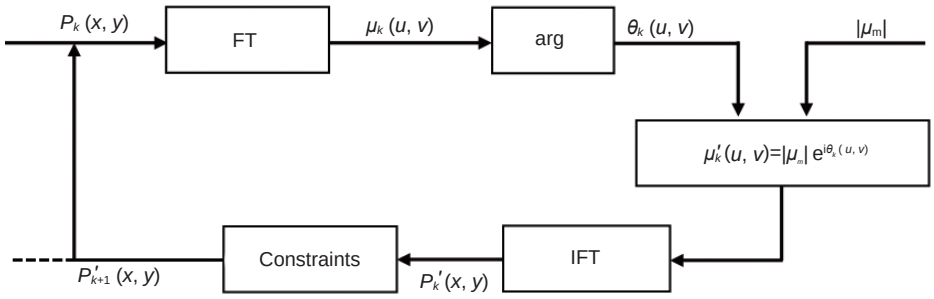

Fig. S1 | Block diagram for an iterative phase recovery algorithm. FT: Fourier transform; arg: phase angle of $\mu_k(u,v)$; $|\mu_m|$: module of the degree of coherence of SMPCBs (measured from experiment or known in advance); IFT: inverse Fourier transform; Constraints: real space constraints to calculate P_{k+1} out of P_k.

There are multiple ways to implement this constraint into the algorithm. The first implementation is known as the 'Error-Reduction' algorithm and sets

$$P_{k+1}(x,y) = \begin{cases} P_k'(x,y) & \text{for } (x,y) \notin \Gamma, \\ 0 & \text{for } (x,y) \in \Gamma. \end{cases} \tag{S23}$$

Another possible implementation is called the 'Hybrid Input-Output' algorithm and defines

$$P_{k+1}(x,y) = \begin{cases} P_k'(x,y) & \text{for } (x,y) \notin \Gamma, \\ P_k(x,y) - \beta P_k'(x,y) & \text{for } (x,y) \in \Gamma, \end{cases} \tag{S24}$$

where β is a feedback parameter that control the convergence properties of the algorithm. When $P_{k+1}(x, y)$ is calculated it can be used as the starting point for the $(k+1)^{\text{th}}$ iteration.

The convergence of the algorithms is monitored by calculating the squared error E_k^2 between the autocorrelation of the retrieved image with the measured one

$$E_k^2 = \left[|FT(P_k')| - |\mu_m| \right]^2. \tag{S25}$$

Consistently with the scheme already suggested in ref.[3,4], the best convergence is by starting with the Hybrid Input-Output algorithm and gradually lowering β from 2 to 0 in steps of 0.05 and running 10 iteration per value of β. Then we run 100 iterations with the Error-Reduction algorithm to reduce any residual noise from the image.

Section 3: Simulation approach for the Schell-model partially coherent beams with a cross-phase in turbulent atmosphere

In our simulation, a Schell-model partially coherent beam source (SMPCBs) with a cross-phase (CP) is decomposed as a series of random electric fields (each represents as a realization), with the help of the complex screen method. After that, the random electric fields passing through the turbulent atmosphere is studied through the multi-phase screen method. Hereto, we introduce the complex screen method and multi-phase screen method in part I and part II, respectively.

Part I. Representations of any genuine SMPCBs with a CP via the complex screen method

At present, there are many literatures reported on the representation of a genuine SMPCBs with a CP via the complex screen method[5,6]. Here we briefly introduce this method, and more relevant details could be found in ref.[5,6]. For a physically genuine SMPCBs with a CP, its CSD function can be alternatively represented as the following integral form

$$\begin{aligned} W_0(\boldsymbol{r}_1, \boldsymbol{r}_2) &= \tau(\boldsymbol{r}_1)\, \tau^*(\boldsymbol{r}_2)\, \mu_0(\Delta \boldsymbol{r}) \exp\left[\mathrm{i}u(x_1 y_1 - x_2 y_2)\right] \\ &= \tau_n(\boldsymbol{r}_1)\, \tau_n^*(\boldsymbol{r}_2) \int P(\nu_1, \nu_2) \exp\left[-\mathrm{i}k(\nu_2 \cdot \boldsymbol{r}_2 - \nu_1 \cdot \boldsymbol{r}_1)\right] \mathrm{d}^2\nu_1 \mathrm{d}^2\nu_2, \end{aligned} \tag{S26}$$

with

$$\tau_n(\boldsymbol{r}) = \tau(\boldsymbol{r}) \exp(\mathrm{i}uxy),$$

$$P(\nu_1, \nu_2) = \sqrt{P(\nu_1)}\sqrt{P(\nu_2)}\,\delta(\nu_1 - \nu_2), \tag{S27}$$

where $\tau_n(\boldsymbol{r})$ as the new complex function, determines the source intensity profile $I=|\tau_n(\boldsymbol{r})|^2$. $P(\boldsymbol{\nu})$ as the power spectral density is a non-negtive function, and δ denotes the Dirac function, which can be rewritten as

$$\delta(\boldsymbol{\nu}_1 - \boldsymbol{\nu}_2) = \langle C_n(\boldsymbol{\nu}_1)\, C_n^*(\boldsymbol{\nu}_2) \rangle, \tag{S28}$$

here $C_n(\boldsymbol{\nu})$ (n = 1, 2, 3,...) denotes the random complex function whose probability density functions of amplitude and phase of $C_n(\boldsymbol{\nu})$ obey the negative exponent and uniform distribution, respectively. The angular bracket stands for the ensemble average. We assume the field is statistically stationary. On substituting Eqs. S27 and S28 into S26, Eq. S26 are rewritten as

$$W_0(\boldsymbol{r}_1, \boldsymbol{r}_2) = \langle E_{n0}(\boldsymbol{r}_1)\, E_{n0}^*(\boldsymbol{r}_2) \rangle \approx \frac{1}{N} \sum_{n0=1}^{N} E_{n0}(\boldsymbol{r}_1)\, E_{n0}^*(\boldsymbol{r}_2), \tag{S29}$$

with

$$E_{n0}(\boldsymbol{r}) = \tau_n(\boldsymbol{r}) \times T_{n0}(\boldsymbol{r}), \tag{S30}$$

where $E_{n0}(\boldsymbol{r})$ denotes one realization of random electric fields. $T_{n0}(\boldsymbol{r}) = FT\left[\sqrt{P(\boldsymbol{v})} \times C_n(\boldsymbol{v})\right]$ is the one random complex screen with FT standing for the Fourier transform. Therefore, the generation of the SMPCBs can be treated as the fully coherent portion $[\tau_n(\boldsymbol{r})]$ illuminates the random complex screens $[T(\boldsymbol{r})]$. Hence, this method is named the complex screen method.

Part II. Computational propagation model (multi-phase screen method) for the SMPCBs with a CP propagating in turbulent atmosphere

In the above part, we have produced the random electric fields via the complex screen method. These fields are treated as the source beam, who will pass the turbulent atmosphere. The multi-phase screen method is widely used for numerically simulating the propagation of light beams through turbulent atmosphere[7,8]. We briefly outline here as well, and more relevant details could be found in ref.[7,8]. In this method, the turbulence is modeled as a collection of thin random phase screens with the desired turbulence statistics. Phase screens are placed along the propagation path at equal intervals $\Delta z = z/N_{\mathrm{T}}$, shown in Fig. S2. Δz is the distance between two adjacent phase screens, z is the overall propagation distance, and N_{T} is the total number of screens.

The scenario for simulating the propagation of SCPCBs with a CP in atmospheric turbulence is as follows. The incident electric field of the source $E^1(\boldsymbol{r}_1)$ propagates a distance Δz in free space, and arrives at the first phase screen. Then, the electric field turns to be $\bar{E}^1(\boldsymbol{r}_2)$, which can be derived with the help of the Huygens-Fresnel principle. It will be modulated by the random phase screen that represents the accumulated turbulence effect over the distance Δz, i.e., $E^2(\boldsymbol{r}_2) = \bar{E}^1(\boldsymbol{r}_2)\exp[\mathrm{i}\theta_1(\boldsymbol{r}_2)]$, where θ_1 is the accumulated phase fluctuations induced by the turbulence over the distance Δz. The following propagation steps just repeat the first propagation step, until the beam reaches the last phase screen. The incident electric field is expressed as $E^{n+1}(\boldsymbol{r}_{n+1}) = \bar{E}^n(\boldsymbol{r}_{n+1})\exp[\mathrm{i}\theta_n(\boldsymbol{r}_{n+1})]$. Finally, the light field is focused by a collecting lens and arrives at the detector in the receiver plane.

The method for synthesizing θ_n is similar to that for the synthesis of the complex screen described above but uses the power spectrum $\Phi_n(\boldsymbol{\kappa})$ of the turbulence-induced refractive index fluctuations. The relationship between the power spectrum of the turbulence and the spectrum $\Phi_\theta(\boldsymbol{\kappa})$ of the phase screen induced by turbulence is given by the following formula,

$$\Phi_\theta(\boldsymbol{\kappa}) = 2\pi\Delta z k^2 \Phi_n(\boldsymbol{\kappa}) \ , \tag{S31}$$

where $k = 2\pi/\lambda$ denotes the wavenumber of a light wave with the wavelength λ; $\boldsymbol{\kappa} \equiv 2\pi(f_x, f_y)$ is the spatial frequency vector. Following the same procedure for synthesis of the complex screen for partially coherent beams, Eq. (S31) is first

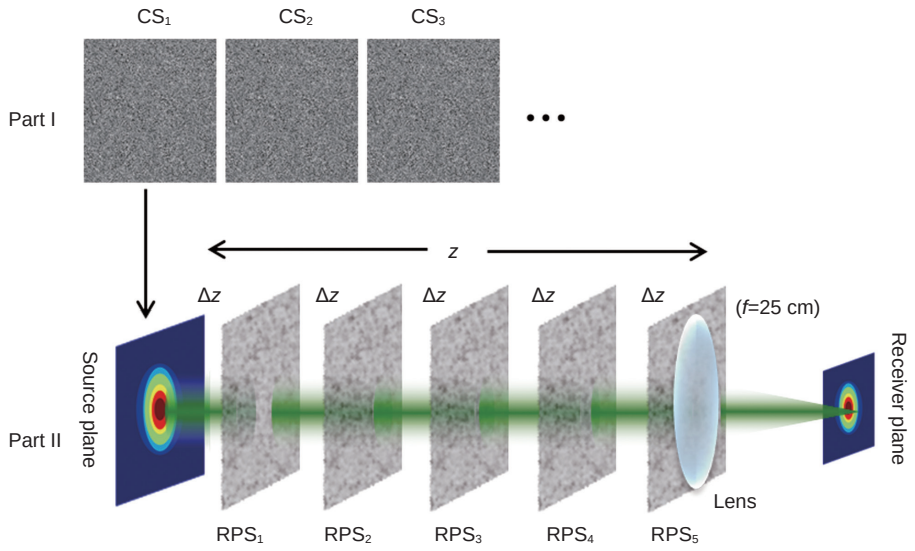

Fig. S2 | Computational propagation model (phase screen method) for a SMPCBs with a CP generating and propagating in turbulent atmosphere. Part I: Three typical realizations of the modulus of the complex screens (CSs). RPS: random phase screen.

multiplied by a random complex function $C_n(\boldsymbol{\kappa})$; we take a Fourier transform of the result. The real or imaginary parts of the result each represent a valid realization of the turbulence screen phase, e.g. $\theta_n(\boldsymbol{r}_{n+1}) = \mathrm{Re}\{FT[C_n(\boldsymbol{\kappa})\times\Phi_\theta(\boldsymbol{\kappa})]\}$, where Re represents the real part.

In our simulation, the von Kármán spectrum is adopted as the power spectral density of turbulence, which reads as

$$\Phi_n(\boldsymbol{\kappa}) = 0.33C_n^2(\kappa^2+\boldsymbol{\kappa}_0^2)^{-11/6}\exp(-\boldsymbol{\kappa}^2+\kappa_m^2)\,, \tag{S32}$$

where C_n^2 is the structure constant of turbulence; κ_m =5.92l_0 with l_0 being the inner scale, and $\kappa_0 = 2\pi/L_0$ with L_0 being the outer scale. The turbulence and beam parameters are chosen to be l_0 = 1.0 mm, L_0 = 1.0 m, and λ = 532 nm. Further, the propagation distance is set to be z = 1 m and the total of 5 phase screens are applied in our simulation.

References

1. Fienup JR. Reconstruction of an object from the modulus of its Fourier transform. *Opt Lett* **3**, 27–29 (1978).
2. Fienup JR. Phase retrieval algorithms: a comparison. *Appl Opt* **21**, 2758–2769 (1982).
3. Bertolotti J, van Putten EG, Blum C, Lagendijk A, Vos WL et al. Non-invasive imaging through opaque scattering layers. *Nature* **491**, 232–234 (2012).
4. Katz O, Heidmann P, Fink M, Gigan S. Non-invasive single-shot imaging through scattering layers and around corners via speckle correlations. *Nat Photonics* **8**, 784–790 (2014).
5. Voelz D, Xiao XF, Korotkova O. Numerical modeling of Schell-model beams with arbitrary far-field patterns. *Opt Lett* **40**, 352–355 (2015).
6. Ma PJ, Kacerovská B, Khosravi R, Liang CH, Zeng J et al. Numerical approach for studying the evolution of the degrees of coherence of partially coherent beams propagation through an ABCD optical system. *Appl Sci* **9**, 2084 (2019).
7. Yu JY, Huang Y, Wang F, Liu XL, Gbur G et al. Scintillation properties of a partially coherent vector beam with vortex phase in turbulent atmosphere. *Opt Express* **27**, 26676–26688 (2019).
8. Martin JM, Flatté SM. Intensity images and statistics from numerical simulation of wave propagation in 3-D random media. *Appl Opt* **27**, 2111–2126 (1988).